OPEN ACCESS
IOP Publishing
Superconductor Science and Technology
Supercond. Sci. Technol. **38** (2025) 035012 (12pp)
https://doi.org/10.1088/1361-6668/adaf5c

A compact conduction cooled flux pump operating below 77 K

Muhammad H Iftikhar, Ercan Ertekin, Min Zhang* and Weijia Yuan

Applied Superconductivity Laboratory, Department of Electronic and Electrical Engineering University of Strathclyde, G1 1XW Glasgow, United Kingdom

E-mail: min.zhang@strath.ac.uk

Received 15 August 2024, revised 19 December 2024
Accepted for publication 28 January 2025
Published 11 February 2025

Abstract

High-temperature superconducting (HTS) magnets are widely used in high field applications due to their exceptional current-carrying capabilities. Traditionally, these magnets are powered by high current power supplies via current leads, which complicates insulation between cryogenic and room temperature environments and introduces significant heat leaks. Recent advancements in flux pumps for HTS magnets now allow charging currents in the kA range without the need for traditional power supplies. However, while some research has realized conduction-cooled traveling wave HTS flux pumps, much of the focus for transformer rectifier flux pumps remains on operating them to charge magnets at liquid cryogen temperatures, with limited attention given to the heat load and cooling capabilities of modern dry cryocoolers. This study presents a compact, modular flux pump designed for operation in conduction-cooled environments. It examines the impact of cooling power on the flux pump's performance in such settings. A lumped element model implemented in PLECS is validated through experiments conducted at 70 K and 30 K, demonstrating consistent results. Based on this validation, we demonstrate the capability to charge an HTS magnet to 300 mT (≈800 A) in a conduction-cooled environment using a compact, self-regulating HTS flux pump.

Keywords: flux pump, HTS, magnet, superconductors

1. Introduction

In recent years, advancements in high-temperature superconducting coated conductors (HTS-CCs) have greatly improved their performance and cost-efficiency, achieving higher critical temperatures and increased current-carrying capabilities [1, 2]. Improvements in HTS tapes have opened up a wide range of industrial applications and commercial products. HTS magnets, in particular, show strong potential, offering high critical current densities at higher magnetic fields and operating temperatures, making them promising for various applications [3–6].

However, maintaining a stable current in HTS magnets presents unique challenges due to effects like magnetic flux creep and joint resistance, which prevent achieving the persistent current seen in low-temperature superconductors [7]. To address these issues, a current stabilization system is needed to counteract continuous current losses. Conventional power supplies and current leads limit HTS magnet performance by introducing excess heat [8, 9], which strains the cooling system. Traditionally, HTS magnets have relied on direct power supply methods, but the current leads connecting room temperature and cryogenic environments create additional heat

* Author to whom any correspondence should be addressed.

leakage, raising cooling costs. Additionally, using a DC power source for HTS magnets can be expensive.

In 1966, a concept of DC transformer is explored [10], using quantum rectification to convert alternating magnetic fields into a DC component. This concept inspired the development of flux pump technology, a wireless energy transfer method that generates DC currents in HTS tapes by applying discrete magnetic fields. Flux pumping has emerged as an efficient, adjustable, and cost-effective solution to excite and stabilize HTS magnets, offering great promise for enhancing HTS magnet performance [11–16].

Flux pumping techniques provide an effective solution for addressing current decay in HTS magnets by enabling wireless current compensation [17]. This method supports a quasi-persistent current mode with minimal heat leakage into the cryostat [18], significantly improving system efficiency. With this approach, HTS magnets can be designed to achieve nearly persistent current operation, opening up new possibilities. This article explore the charging of HTS magnets via a self-rectifying HTS flux pump. Although recent devices have reached currents above 1 kA, they are primarily designed for liquid cryogen environments [19]. There are a few experiments on conduction-cooled HTS dynamo and pulse-type flux pump [20, 21], however, there is a lack of study for self-switching flux pump under conduction-cooled conditions. Here, we present a self-rectifying HTS flux pump that operates at both 77 K and 30 K, examining electrical and thermal challenges. This work is supported by both simulation and experimental results, providing a foundation for future applications in conduction-cooled environments.

2. Proposed HTS flux pump system

2.1. HTS magnet

The HTS Magnet is designed to be cooled using conduction cooling. The magnet's former is made from oxygen-free brass, measuring 10 mm in thickness and 70 mm in diameter. A 8 meters of HTS tape is wound into a double pancake coil forming an HTS magnet. The resulting magnet had an inductance of 32 μH and a critical current of 160 A at 77 K, measured using the criteria $E_0 = 10^{-4}$ V·m^{-1}, and the field measured at the center is 62 mT. The HTS magnet is provided with two copper terminals where the charging coil is connected. The HTS tape from the double pancake coil is extended 45 cm in length to form the bridge, with one side passed through an S-shaped slit in the bridge former to change its direction. The resulting bifilar bridge is wound over the former, as figure 1(a) depicts. The former for the bridge, which is 12 mm thick and 120 mm in diameter, is housed on top of the magnet. The large diameter of the bridge minimizes the effect of the magnet's field on the critical current density ($\mathbf{J}_c$) of the bridge. The magnet, bridge, and terminals are housed in a cup-shaped container. This design integrates the bridge as part of the magnet, resulting in a compact HTS magnet as illustrated in figure 1(b).

2.2. Charging coil

The excitation circuit features a transformer with a 300:1 transformation ratio, utilizing copper on the primary side and HTS tape on the secondary side. The transformer was fabricated using amorphous cut cores from Hitachi metals, which exhibit low core losses and high saturation flux density (B_s = 1.56 T). To serve as a charging coil, two HTS tapes were wound in parallel to create a 1-turn secondary coil with a critical current of 600 A per tape. The charging coil is housed in an oxygen-free brass former, designed for conduction cooling, and equipped with copper terminals for connection to the magnet as shown in figure 1.

2.3. Impregnation of HTS magnet and charging coil

The HTS magnet and charging coil are housed in a brass former and it is crucial to distribute cooling evenly across the superconductor, including portions not in direct contact with the former. In this study, conduction cooling is used, making impregnation a crucial aspect in achieving a cooling temperature of 30 K. Previous research by Kandasamy *et al* showed that phase change materials provide an effective heat sink with improved thermal performance in [22]. Ideal phase change materials possess high thermal conductivity, high specific heat and density, long-term durability, and reliable freezing behavior. Among various classes of phase change materials, paraffin waxes are most common and widely used. Matusuda *et al* in [23] found that paraffin impregnation effectively prevents degradation of the HTS magnet. In this work, paraffin wax with a melting temperature of 55 °C was selected for impregnating the HTS magnet and charging coil due to its high latent heat values (145–240 kJ kg^{-1}) and chemical stability. The main challenge in using paraffin wax was its low thermal conductivity (below 0.1 W (m·K)$^{-1}$). To address this issue, ceramic fillers were added to enhance the thermal conductivity of the paraffin wax mixture. Aluminium nitride (AIN) with particle size less than 10 microns was chosen as the ceramic filler due to its high thermal conductivity, excellent electrical insulation, low density, low thermal expansion, superior resistivity against thermal shock, and relative economy as reported by Badakhsh *et al* in 2017 [24]. A concentration of fillers greater than 3% was found to improve the thermal conductivity by more than 18% and thermal responsivity by over 28% [25, 26]. This improved heat transfer from and to the paraffin wax allowed for the sample to be cooled down to 30 K. The mixture was prepared at 60 °C with continuous stirring, with a ratio of 10:1 between paraffin wax and AIN. After thorough mixing, the mixture was placed in a degassing chamber to eliminate any bubbles, as air pockets in the magnet could compromise its thermal conductivity.

2.4. HTS flux pump system

The HTS magnet and charging coil are securely mounted into a specially designed frame fixture, customized to fit onto the

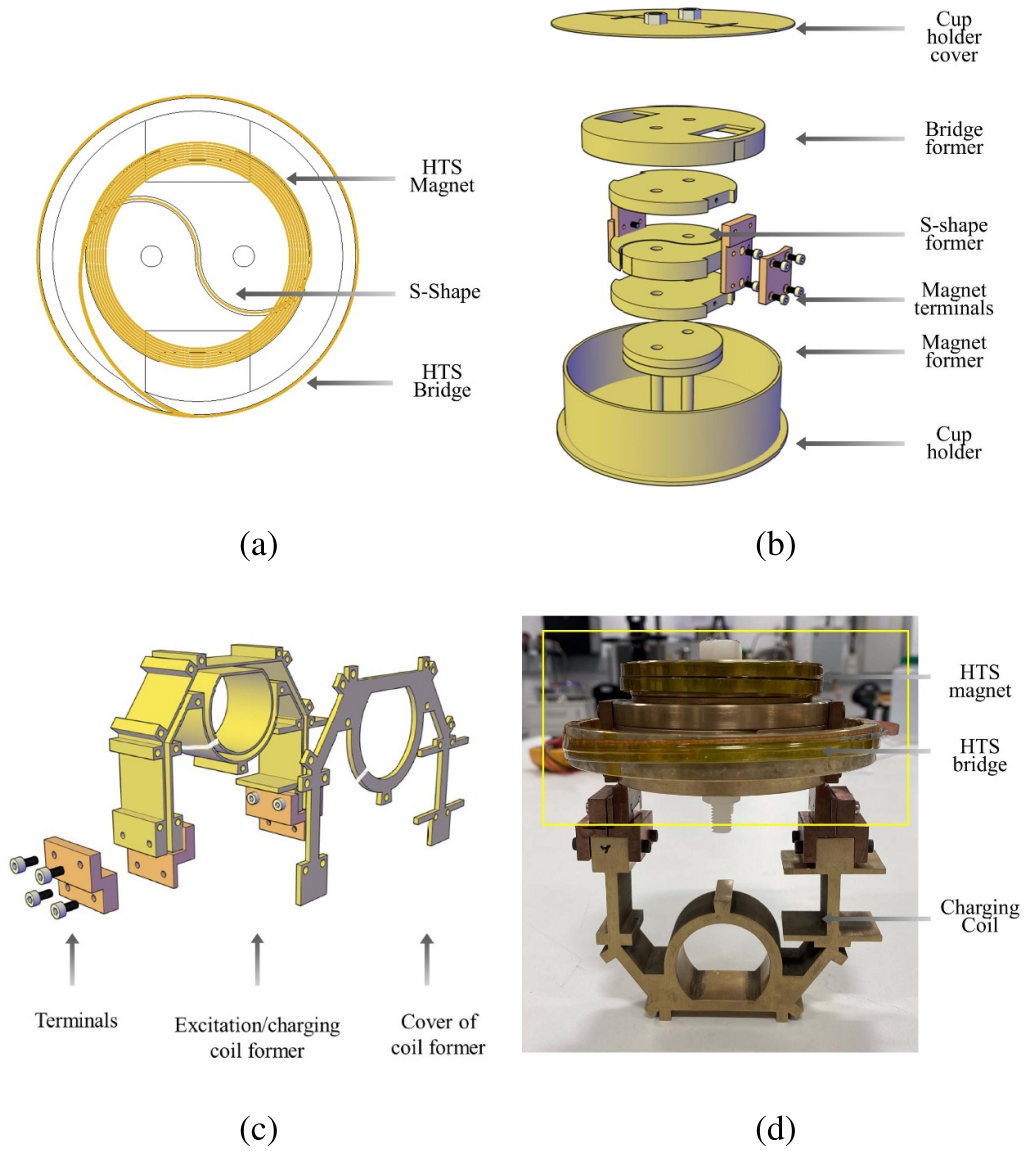

Figure 1. (a) The HTS magnet and bridge superconductor configured in a bifilar pancake configuration with direction change via an S-shaped slit in the former. (b) 3D exploded diagram of the HTS magnet former highlighting its components and design configuration. (c) Exploded diagram of charging coil former: showcasing components and terminals with adjoining bolts. (d) The yellow box depicts the HTS magnet, while the bottom section shows the charging coil.

cooling plate of the cryostat. The fixture is engineered with a sturdy support at the bottom to hold the transformer in place, allowing it to efficiently induce current into the secondary coil as illustrated in figures 2(a) and (b).

To facilitate precise measurement of the magnetic field, the HTS magnet is preinstalled with a GHS-C Cryogenic 1D Hall sensor. The temperatures are monitored using two PT100 temperature sensors, one located on the magnet bridge and the other on the charging coil. Furthermore, to measure the induced current, a current transducer has been incorporated into the design of the charging coil. Finally, the 30 K flux pump is securely installed on the cooling plate in the cryostat, as illustrated in figure 2(c), completing the setup process.

3. Simulation and experiment

3.1. Equivalent circuit model

The circuit diagram of the flux pump system is presented in figure 3. The magnet and charging coil are designed with copper terminals to facilitate connections. The resistance introduced by these terminals, which eliminates the DC component in the charging coil, is denoted as R_{cu} and is approximately $7 \times 10^{-5}\,\Omega$. The HTS-CC of the magnet extends beyond the magnet terminals and is soldered together to form a bifilar bridge. In this context, R_j represents the soldering joint in the bridge, which is approximately $1 \times 10^{-5}\,\Omega$, R_{ff} represents the flux flow resistance of the bridge superconductor, and L_m rep-

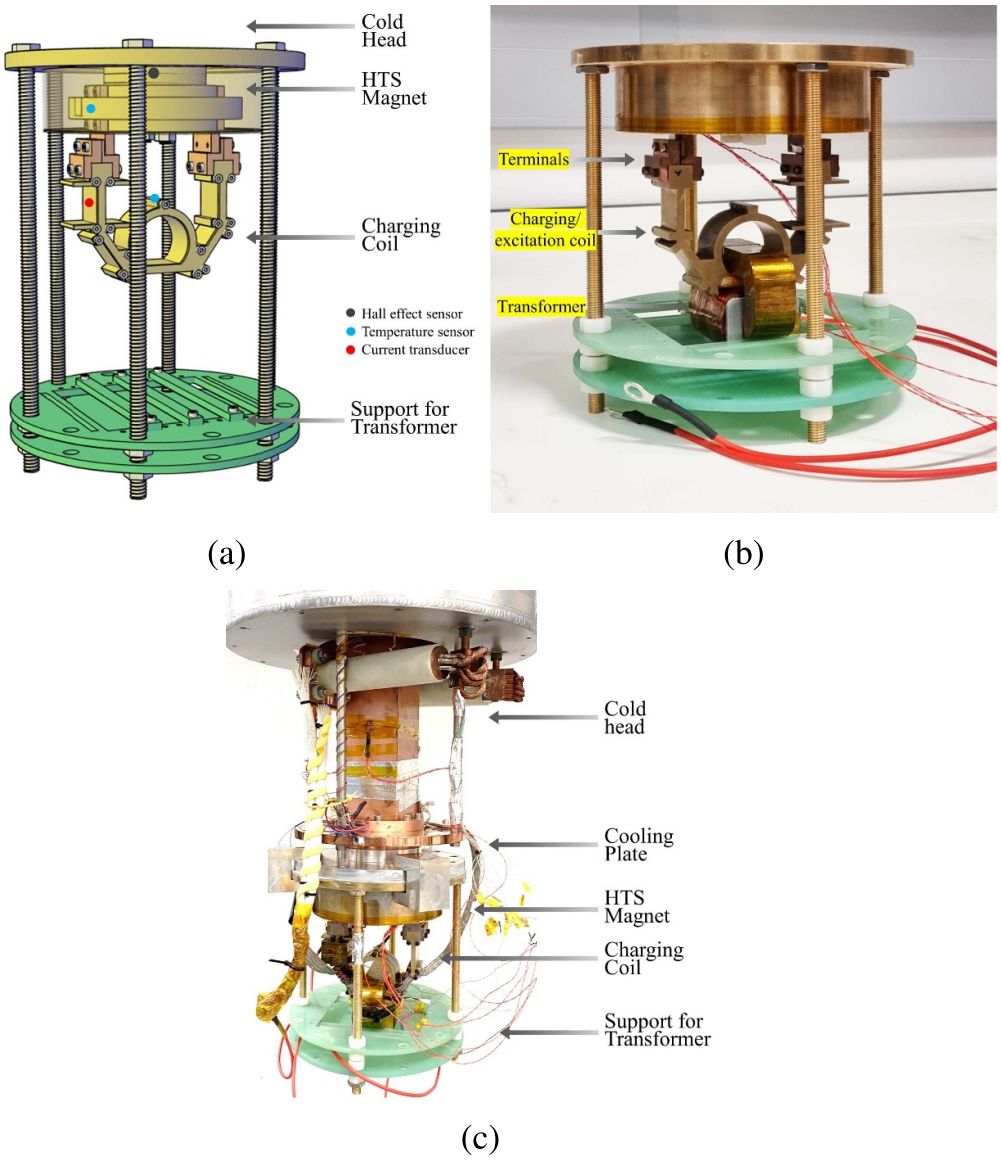

Figure 2. (a) Schematic diagram of the final assembly of 30 K HTS flux pump. (b) Final assembly image showcasing transformer, HTS secondary/charging coil and HTS magnet. (c) Image of HTS flux pump installed on cryostat cold head for operation at 30 K.

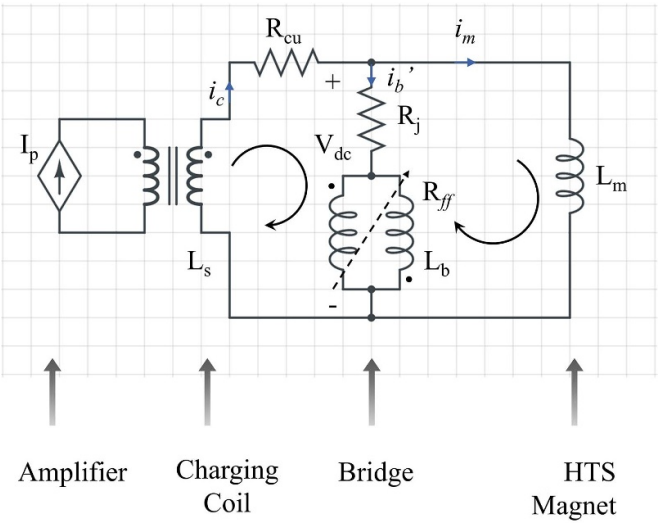

Figure 3. The equivalent circuit of the flux pump, which includes the charging coil, bifilar bridge, and magnet.

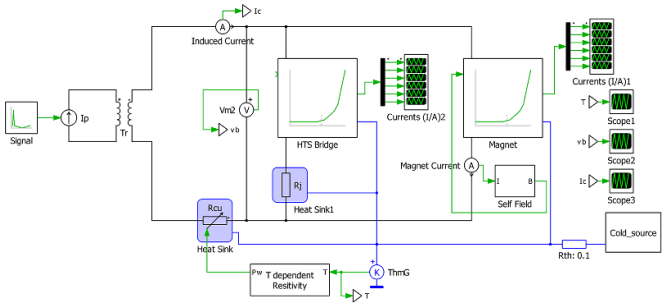

Figure 4. The equivalent circuit of the flux pump, which includes the charging coil, bifilar bridge, and magnet.

resents the inductance of the HTS magnet. It is worth noting that since the bridge is constructed in a bifilar manner, it has negligible inductance.

The induced current in the charging coil can be calculated using the following equation presented below.

$$0 = \frac{\mathrm{d}\phi}{\mathrm{d}t} + L_\mathrm{s}\frac{\mathrm{d}i_\mathrm{c}}{\mathrm{d}t} + i_\mathrm{c}R_\mathrm{cu} + i_\mathrm{b}Z_\mathrm{b} + i_\mathrm{b}R_\mathrm{j}. \tag{1}$$

The flux generated by the primary copper of the transformer is coupled with HTS charging coil. The charging current is denoted by i_c, and the inductance of the charging coil is represented by L_s. R_j is used to denote the joint resistance, and Z_b represents the bridge impedance. Since the bridge inductance is negligible, the corresponding term can be approximated to zero. During the first cycle, the load current is zero, and thus, the current flowing through the bridge, represented by i_b, is equal to i_c. However, after the flux pumping action, the flux starts to accumulate in the magnet, and the DC current begins flowing through the bridge, resulting in a gradual increase in the charging current.

In an ideal transformer, the secondary charging current (i_c) is always proportional to the primary current (i_p). However, in a real transformer, if the load impedance (Z_b) is high, the output voltage may reach its limit, causing the secondary current to limit the primary current. A transformer comprising of HTS as its secondary, there is a voltage limit, which occurs when the current flowing through the HTS tape exceeds its critical value and causes it to quench. In this section, we will discuss the voltages induced across the bridge superconductor, the mathematical expression for dc voltages across the bridge can be given as,

$$V_\mathrm{dc} = i_\mathrm{b}R_\mathrm{j} + i_\mathrm{b}R_\mathrm{d}ff + L_\mathrm{b}\frac{\mathrm{d}i_\mathrm{b}}{\mathrm{d}t} = L_\mathrm{m}\frac{\mathrm{d}i_\mathrm{m}}{\mathrm{d}t}, \tag{2}$$

where V_dc, is the positive voltage across the bridge, in (2) for a bifilar bridge the L_b is zero so the dc voltages V_dc across the bridge is purely due to flux flow resistivity R_ff.

3.2. Simulation results for 77 K

A PLECS simulation model is built based on the circuit presented in figure 3. The temperature and field-dependent HTS CC J_c(T,B) is modeled to represent both the magnet and the bridge. The magnet inductance is set to 32 μH, and since the bridge is in a bifilar configuration, its inductance is set to zero as illustrated in figure 4.

The copper terminal resistance is modeled using a lookup table approach, where the temperature-dependent resistivity of copper is utilized [27, 28]. A thermal resistance of 0.1 K W^{-1} is used in the thermal network. The cold head is implemented using a controlled heat flow source to remove heat from the circuit. To replicate the cold head capacity, a lookup table is created based on the graph illustrated in figure 7(b), and a PID controller is used to control the heat flow source.

A charging current with an amplitude of 460 A is induced in the charging coil shown in figure 5(a), producing a voltage of 28 mV across the bridge and injecting flux into the magnet shown in figure 5(b). The bridge voltage becomes biased in the negative direction as the magnet current increases, eventually saturating just below 60 mT as shown in figure 5(c).

There was no significant change in the temperature of the flux pump system, as the heat produced by the flux pump was effectively removed by the cold source as illustrated in figure 5(d).

3.3. Simulation results for 30 K

At an operating temperature of 30 K, a charging current of 980 A is induced to drive the bridge superconductor into the flux flow region shown in figure 6(a). It is important to note that a joint in the bridge limits the critical current at this lower temperature. Additionally, the induced current is limited by the high resistance of the copper. Over time, the bridge voltage begins to rise, further limiting the charging current and indicating heat accumulation in the flux pump assembly as illustrated in figure 6(b).

An estimate of the heat generated by the copper terminals suggests that losses across the bridge reaches approximately 18.3 W. Additional heat generation across the bridge itself is an order of magnitude lower than that observed at the copper terminals. It was anticipated that this heat would be removed by the cold source, but due to the thermal volume of the flux pump system, the heat removal was not quick enough to cool it back down to 30 K after each cycle. As a result, the magnet is charged to 160 mT before the bridge starts to quench, as shown in figure 6(c), dissipating the magnet's energy and causing continuous heat buildup in the bridge. The temperature of the flux pump system, depicted in figure 6(d), rises from 30 K to just below 50 K.

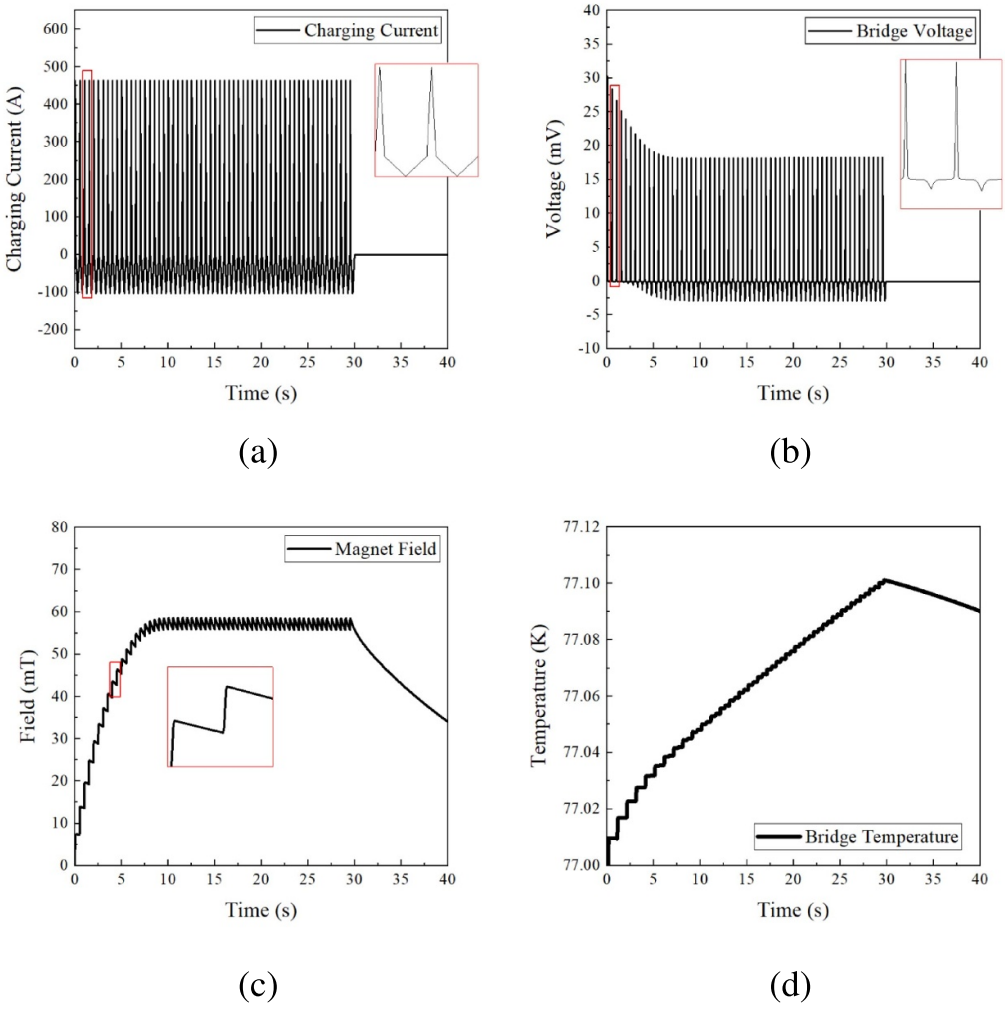

Figure 5. Simulation results at 77 K: (a) Induced current (i_c) in the charging coil. (b) Calculated voltages across the bifilar bridge (V_{dc}). (c) Magnetic field at the center of the magnet. (d) Temperature of the bridge superconductor.

3.4. Experimental setup

The cooling system utilized in this study is based on the principle of conduction cooling and is capable of reaching temperatures as low as 20 K. The system, presented in figure 7(a), consists of a vacuum-sealed cryostat produced by ICE Oxford, which is fitted with a CH-110 cold head by Sumitomo. The capacity waveform is illustrated in figure 7(b). The helium compressor is designed to deliver high-pressure oil-free helium gas to the cryogenic refrigerators. Additionally, the system includes a water chiller, a turbo molecular vacuum pump by Pfeiffer capable of reaching 10^{-7} hPa within the cryostat, and finally, the 336 temperature controller by Lakeshore with four channels and built-in PID control, which plays a crucial role in maintaining and controlling the temperature of the test subject.

3.5. Applied current

An asymmetric signal is used as the primary input current, as illustrated in figure 8. The positive peak is maintained at a higher value to drive the superconductor into the flux flow region, enabling flux flow from the secondary side to the load side (magnet). Conversely, the negative peak is kept much lower to retain the flux within the load. To eliminate the DC component, the length of the positive period is inversely proportional to the peak values of the negative period. Notably, at 77 K, the applied current amplitude is significantly lower, inducing only 400 A on the secondary side to ensure the bridge current exceeds its critical value. In contrast, at 30 K, a higher current is required to drive the superconductor into the flux flow region. Additionally, the primary winding (copper) of the transformer has an input resistance of 1.1 Ω and an inductance of 110 mH. We employ a power amplifier, AETECHRON 7796 5000 W [29], to deliver the current.

3.6. Experimental results for 77 K

This test is performed at 77 K to verify the performance of the flux pump system at LN2 temperature. A current higher than the critical current of the bridge, i.e. 460 A, is induced in the charging coil at a frequency of 1 Hz, as illustrated in figure 9(a), to drive the bridge superconductor into the flux flow region. The bridge produces a positive voltage across the

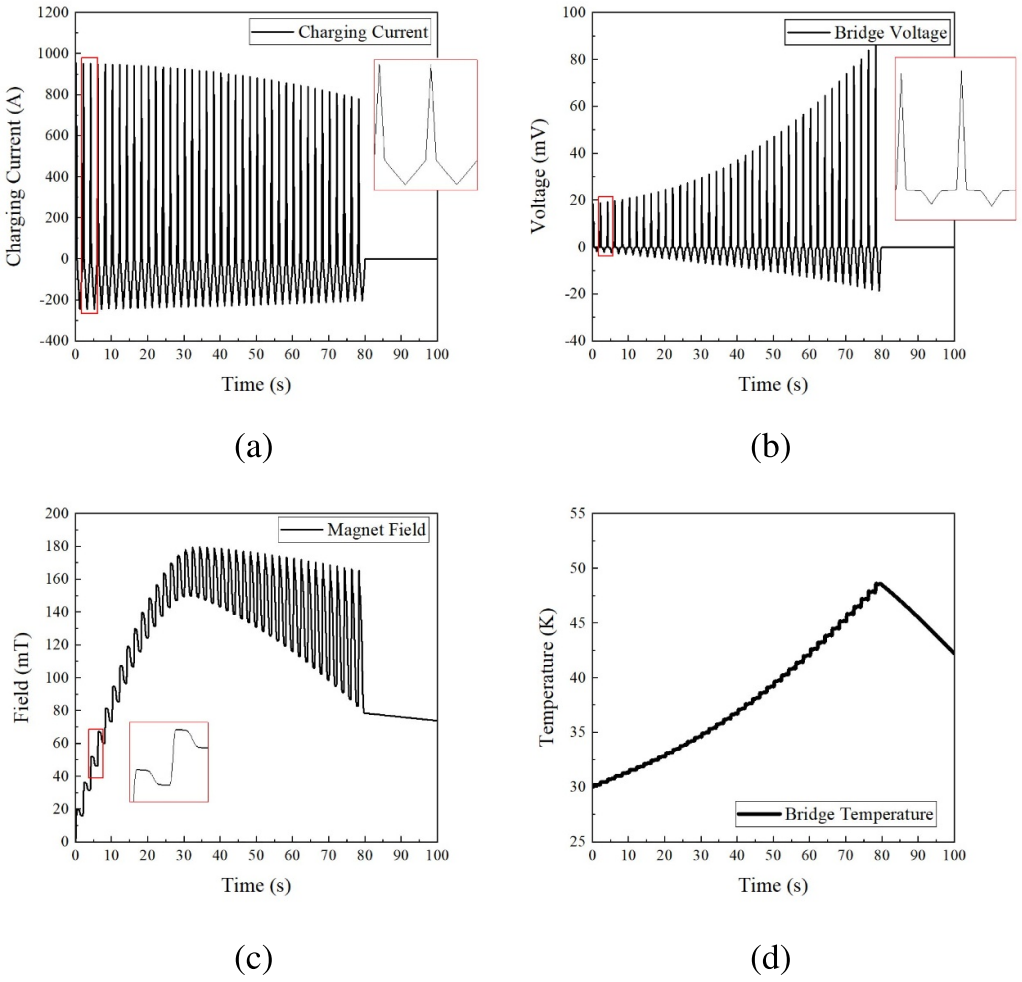

Figure 6. Simulation results at 30 K: (a) induced current (i_c) in the charging coil. (b) Calculated voltages across the bifilar bridge (V_{dc}). (c) Magnetic field at the center of the magnet. (d) Temperature of the bridge superconductor.

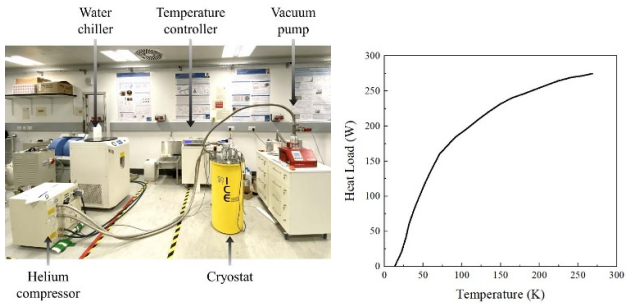

Figure 7. (a) Illustration of the conduction cooling system, showcasing the cryostat, He compressor, temperature controller, turbo molecular pump, and water chiller. (b) CH-110LT Cold Head Capacity Map Using F-70 Compressor at 50 Hz.

magnet, i.e. 32 mV, as shown in figure 9(b), and a small current is injected. The negative cycle retains this current. The amplitude is higher than in the simulation results presented in figure 5(d), which show a smaller peak on the negative side. This difference is due to the ideal source used in the simulation, whereas transients are observed in the experiment. The positive peak is significant as it performs the switching and injects current into the magnet, while the negative peak only serves to remove the DC components from the secondary side, preventing transformer saturation. Over time, this current accumulates, and the magnet is saturated at 60 mT, as shown in figure 9(c).

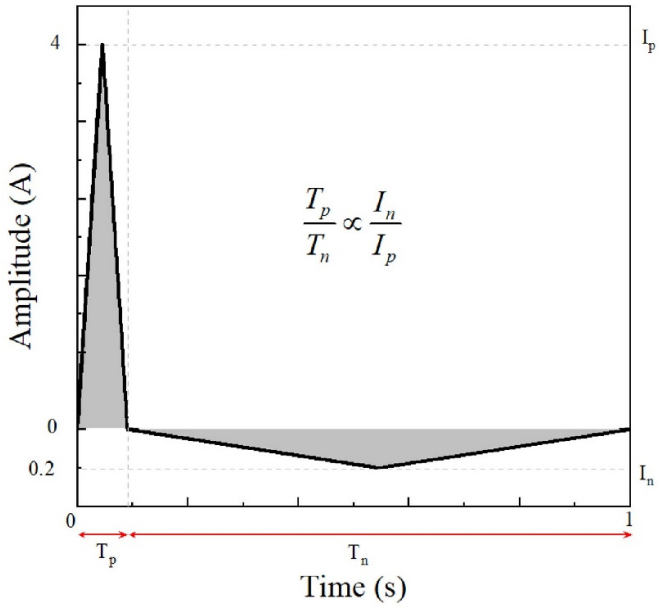

Figure 8. Asymmetric applied current waveform.

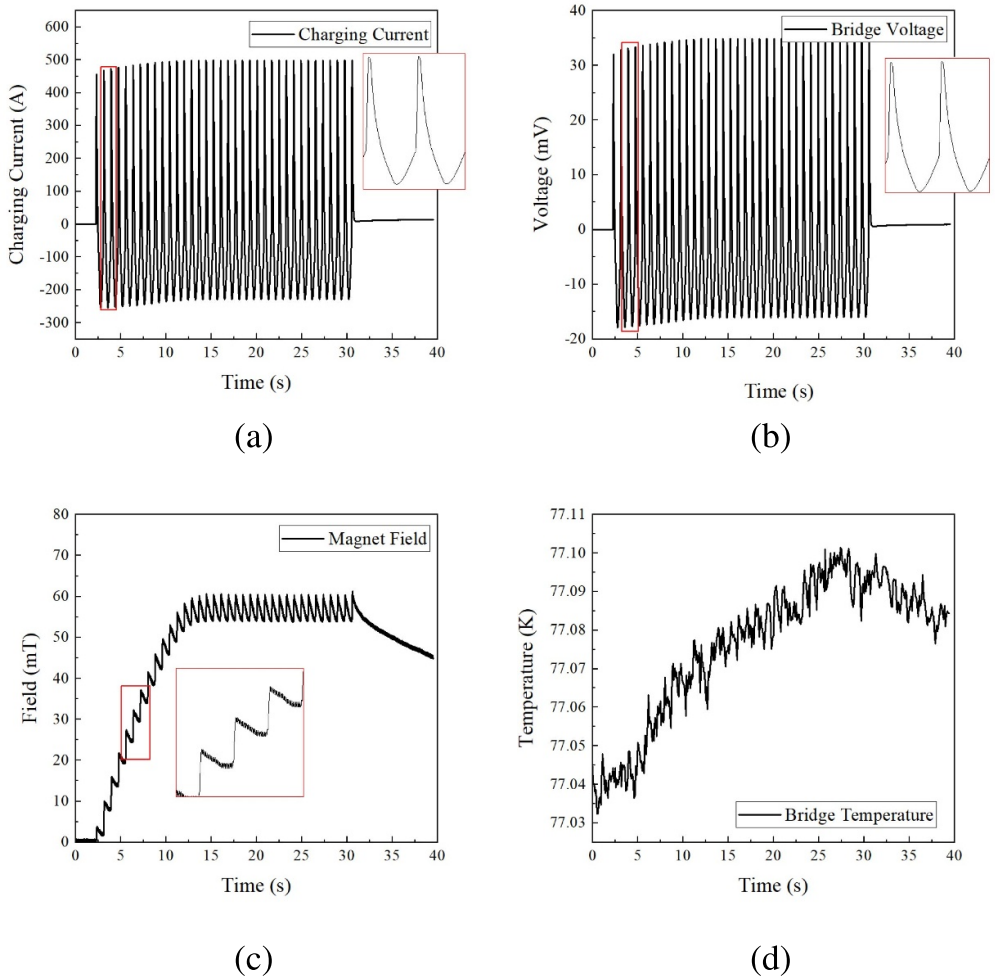

Figure 9. Experiment results at 77 K: (a) induced current (i_c) in the charging coil. (b) Measured voltages across the bifilar bridge (V_{dc}). (c) Magnetic field measured at the center of the magnet. (d) Recorded temperature of the bridge superconductor.

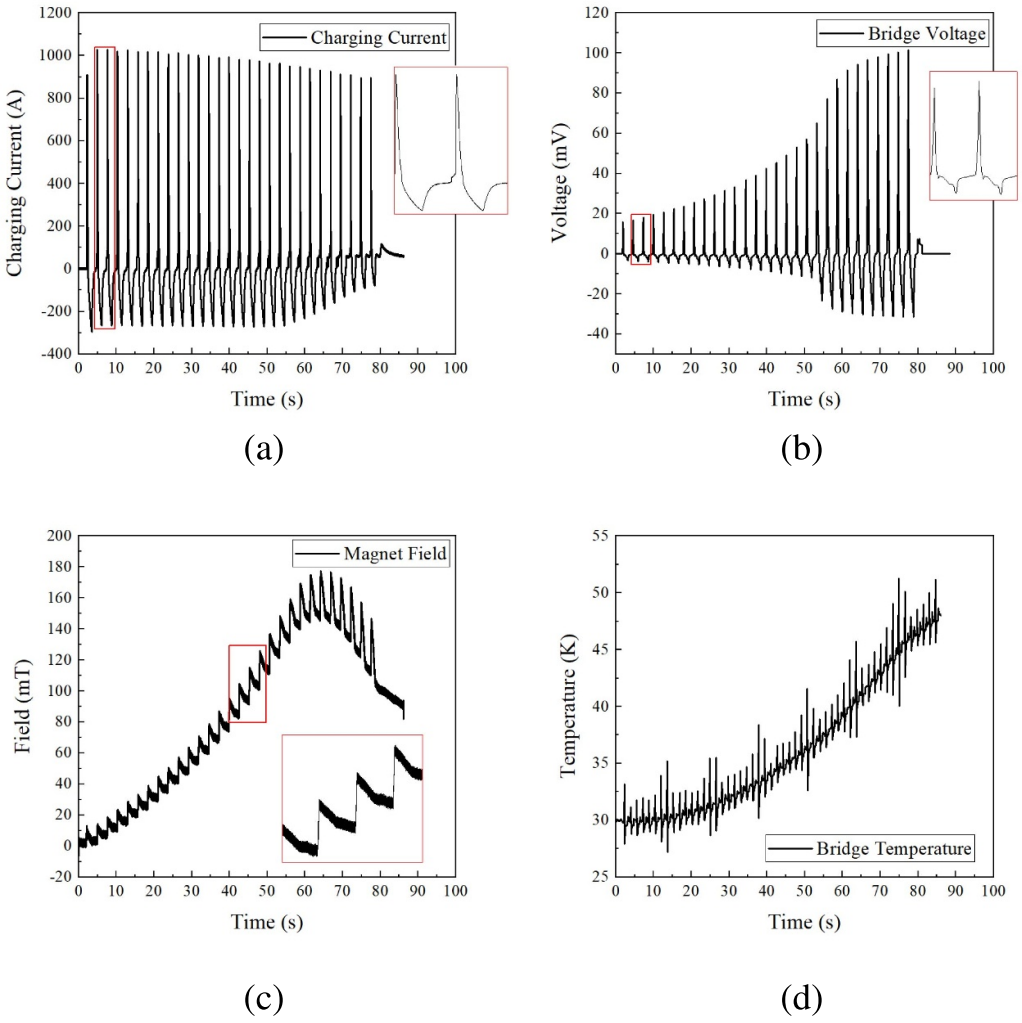

Figure 10. Experiment results at 30 K: (a) induced current (i_c) in the charging coil. (b) Measured voltages across the bifilar bridge (V_{dc}). (c) Magnetic field measured at the center of the magnet. (d) Recorded temperature of the bridge superconductor.

The temperature of the bridge superconductor is closely monitored and recorded, as illustrated in figure 9(d). It was noted that the rise in temperature was not significant and the heat was removed efficiently. It is also worth noting that the cryocooler heat capacity is around 152 W at 77 K.

3.7. Experimental results for 30 K

The cryocooler was further run down to reach the base temperature, but due to the sheer volume of the sample, it struggled to reach 20 K, therefore, the author settled at 30 K. The temperature controller was set to 30 K and operated using a PID controller to maintain the temperature of the flux pump system at 30 K.

Here, the charging current with a peak amplitude of 1 kA is induced in the charging coil at a rate of 0.5 Hz, as illustrated in figure 10(a). The current in the charging coil is limited by the resistance of the copper terminals (R_{cu}). At 30 K, the bridge's critical current is elevated, but due to the presence of the low-resistance face-to-face praying hand tape joint, the charging current was able to drive the bridge superconductor into the flux flow regime. This induced a small positive voltage across the bridge, i.e. 19 mV, as shown in figure 10(b). This bridge voltage successfully injected current into the magnet and retained it during the negative cycle. Over time, the flux started to build up in the magnet, as recorded at the center and illustrated in figure 10(c).

The temperature plot is significant as it continues to rise cycle after cycle. The reason for this harsh temperature rise is the copper terminals R_{cu} at the ends of the bridge coil. Here, R_{cu} plays two roles: first, the copper resistivity does not change as significantly as the conductivity of the HTS, limiting the induced current in the charging coil; and second, it generates heat, which warms up the bridge, continuously reducing the critical current. This can be seen in figure 10(b), where the voltage keeps rising until the point is reached where the induced current starts to quench the bridge. Due to the continuous rise in the bridge voltage, the induced current is limited.

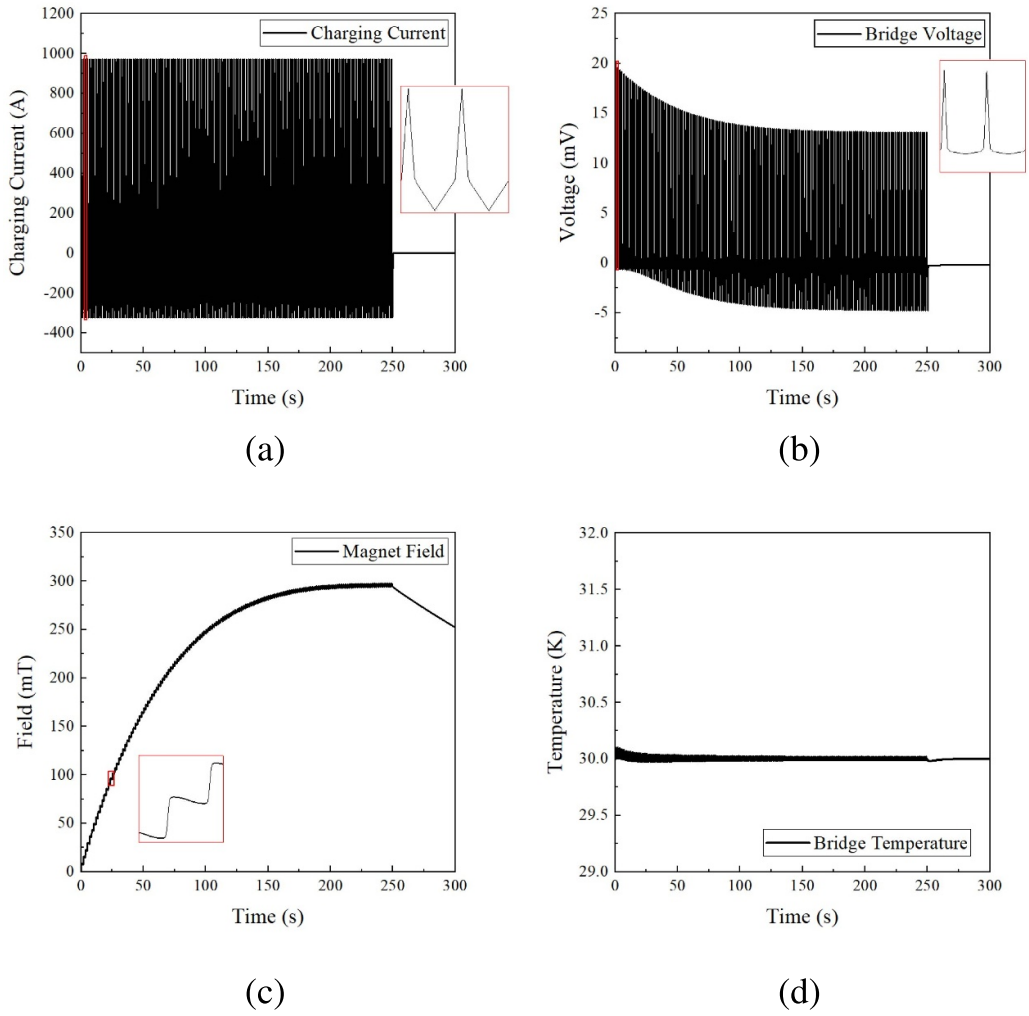

Figure 11. Simulation results at forced cooling to 30 K: (a) induced current (i_c) in the charging coil, (b) calculated voltages across the bifilar bridge (V_{dc}), (c) magnetic field at the center of the magnet, (d) temperature of the bridge superconductor.

In transformer action, if the load impedance is high, the output voltage may reach its limit, so the secondary current cannot follow the primary current [11]. Consequently, we see the flux accumulation in the magnet up to 160 mT, after which the bridge starts to quench and the magnet begins to discharge across it.

This experiment met expectations but also highlighted important aspects of flux pumping in a conduction-cooled environment. At lower temperatures, the cooling capacity of the cryocooler was significantly reduced, and the heat removal was much slower compared to flux pumping operation at 77 K. Although the magnet did not reach its saturation point during flux pumping, the experiment had successful outcomes. First, it proved that flux pumping in HTS magnets is feasible at lower temperatures. Second, it highlighted the need for performance optimization of the resistance in the bridge superconductor, which should be designed in accordance with the operating temperature to avoid current limiting in the secondary side. Lastly, it emphasized the importance of carefully managing the copper mass (thermal management) to minimize heat losses.

4. Discussions

Previously, traveling wave flux pumps, including linear flux pumps [30] and HTS dynamos [20, 31, 32], were primarily operated in conduction-cooled environments to charge coils [21]. The linear motor type flux pumps use a through wall excitation where core extends from room temperature to cold side increasing cooling penalty and cryostat design complication. Where as a dynamo type flux pump requires a moving permanent magnet rotor. A recent study demonstrated that there is a limit to the maximum DC voltage that a dynamo can generate, necessitating complex design configurations to overcome this constraint [16]. However, this article demonstrates a compact modular solution using a self-rectifying

HTS flux pump. This approach offers the advantage of an adjustable bridge construction to generate higher voltages, enabling faster flux pumping into the magnet. The concept is first simulated and the thermal behavior is studied and at 77 K the cooling power was enough to remove the heat generated in the flux pump system. At 30 K, a high current is required to generate the voltage across the bridge to charge the magnet. The higher current generates heat at the copper terminals, which can be mitigated through effective thermal design, such as increasing the copper mass to reduce Joule heating. Furthermore, the terminals not only exposed potential challenges associated with the flux pump but also highlighted opportunities for further research aimed at achieving low-resistivity joints in the assembly. Notably, by either reducing Joule heating of the copper terminals or increasing cooling power to accommodate this heating, the thermal performance of the flux pump can be improved at lower temperatures, as illustrated in figure 11. In this scenario, the same charging current as shown in figure 6 is induced in the charging coil to generate the voltage across the bridge. The key difference from the previous simulation is that the cooling power is adjusted to maintain a temperature of 30 K. The charging current produces a voltage slightly below 20 mV across the bridge, which injects a small current into the magnet, charging it to 300 mT. This is five times higher than the flux injected at 77 K.

5. Conclusion

A compact HTS magnet was designed for conduction-cooled environments, featuring a built-in bifilar bridge for flux pump charging and a detachable charging coil. A PLECS based lumped element model is presented, where temperature and field dependent HTS-CC is modeled. The flux pump is operated at 77 K and 30 K, and the results are then validated with experiments in a conduction cooled cryostat. At 77 K, the flux pump successfully charged the HTS magnet to 60 mT (≈160 A) with no significant temperature increase, mainly due to the high cooling power, which quickly removed the generated heat via the cold head. However, at 30 K, the cooling power of the cold head was noticeably low, resulting in heat accumulation across the bridge. As the temperature gradually increased, the J_c of the bridge started to decrease, leading to a stage where the bridge began to quench, resulting in flux pumping of 160 mT (≈400 A) in the HTS magnet. The heat can be mitigated by using low resistance joints between the charging coil and the HTS magnet or by increasing the cooling power. Further increasing the cooling power allowed the flux pump to charge the HTS magnet to 300 mT (≈800 A).

Data availability statement

The data cannot be made publicly available upon publication because they are not available in a format that is sufficiently accessible or reusable by other researchers. The data that support the findings of this study are available upon reasonable request from the authors.

Acknowledgment

This work was funded by Prof. Min Zhang Royal Academy of Engineering Research Fellowship. Muhammad H Iftikhar acknowledges the John Anderson Research Award for offering a fully-funded studentship at the University of Strathclyde, Glasgow, United Kingdom.

ORCID iDs

Muhammad H Iftikhar https://orcid.org/0000-0001-5537-1827
Min Zhang https://orcid.org/0000-0003-4296-7730
Weijia Yuan https://orcid.org/0000-0002-7953-4704

References

[1] Wang Q *et al* 2021 *Supercond. Sci. Technol.* **35** 023001
[2] Soomro W A, Guo Y, Lu H, Jin J, Shen B and Zhu J 2022 *Energies* **15** 7857
[3] Iwasa Y 2006 *Physica* C **445** 1088–94
[4] Parkinson B 2016 *Supercond. Sci. Technol.* **30** 014009
[5] Zhai Y, van der Laan D, Connolly P and Kessel C 2021 *Fusion Eng. Des.* **168** 112611
[6] Messina G, De Bella E T and Morici L 2019 *IEEE Trans. Appl. Supercond.* **29** 1–5
[7] Seo K and Morita M 2006 *Cryogenics* **46** 354–61
[8] Dresner L 2006 *Stability of Superconductors* (Springer)
[9] Ballarino A 2008 *Physica* C **468** 2143–8
[10] Giaever I 1966 *IEEE Spectr.* **3** 117–22
[11] Geng J and Coombs T 2016 *Supercond. Sci. Technol.* **29** 095004
[12] Rice J H, Geng J, Bumby C W, Weijers H W, Wray S, Zhang H, Schoofs F and Badcock R A 2021 *IEEE Trans. Appl. Supercond.* **32** 1–5
[13] Geng J, Matsuda K, Fu L, Fagnard J F, Zhang H, Zhang X, Shen B, Dong Q, Baghdadi M and Coombs T 2016 *J. Phys. D: Appl. Phys.* **49** 11LT01
[14] Coombs T A, Geng J, Fu L and Matsuda K 2016 *IEEE Trans. Appl. Supercond.* **27** 1–6
[15] Zhang Y, Wang W, Ye H, Wang X, Gao Y, Zhou Q, Liu X and Lei Y 2020 *IEEE Trans. Appl. Supercond.* **30** 1–5
[16] Hamilton K, Pantoja A E, Storey J G, Jiang Z, Badcock R A and Bumby C W 2018 *IEEE Trans. Appl. Supercond.* **28** 1–5
[17] Lee S *et al* 2016 *IEEE Trans. Appl. Supercond.* **26** 1–4
[18] Hoffmann C, Pooke D and Caplin A D 2010 *IEEE Trans. Appl. Supercond.* **21** 1628–31
[19] Geng J, Painter T, Long P, Yang J, Ma J, Dong Q, Shen B, Li C and Coombs T 2019 *Supercond. Sci. Technol.* **32** 074004
[20] Zhai Y, Niu C, Liu X, Wang F, Liu J and Wang Q 2022 *IEEE Trans. Appl. Supercond.* **32** 1–5
[21] Zhai Y, Mu C, Zhu L, Wang J, Li Z, Weng T, Liu J and Wang Q 2023 *IEEE Trans. Appl. Supercond.*
[22] Kandasamy R, Wang X Q and Mujumdar A S 2008 *Appl. Therm. Eng.* **28** 1047–57
[23] Matsuda T, Okamura T, Hamada M, Matsumoto S, Ueno T, Piao R, Yanagisawa Y and Maeda H 2018 *Cryogenics* **90** 47–51
[24] Badakhsh A, Park C W and Kim B J 2017 Preparation and analysis of paraffin-based phase change material using aluminum nitride as the reinforcing agent *4th Int. Conf. on Nanotechnology, Nanomaterials & Thin Films for Energy Applications* (One Central Press, University of Aalto) pp 70–72

[25] El-Sebaii A A, Aboul-Enein S, Ramadan M R I and Shalaby S M 2024 Enhancing the thermal properties of paraffin wax as latent heat storage material using hybrid nanomaterials *Charact. Appl. Nanomater.* **7** 4912
[26] Bose P and Amirtham V A 2016 *Renew. Sustain. Energy Rev.* **65** 81–100
[27] Blondelle F, Sultan A, Collin E and Godfrin H 2014 *J. Low Temp. Phys.* **175** 877–87
[28] Le T, Kim J, Park S and Kim H 2014 *Prog. Supercond. Cryog.* **16** 54–8
[29] Inc AETechron 2024 AETECHRON 7796 industrial amplifier for high current / low impedance operation (available at: https://aetechron.com/product/7796/) (Accessed 02 February 2024)
[30] Lei Y, Long R, Li H, Xiong C, Yang C, Wu C, Yang Z, Tang F and Wang W 2023 *IEEE Trans. Appl. Supercond.* **33** 1–4
[31] Walsh R M, Slade R, Pooke D and Hoffmann C 2013 *IEEE Trans. Appl. Supercond.* **24** 1–5
[32] Hoffmann C, Walsh R, Karrer-Mueller E and Pooke D 2012 *Phys. Proc.* **36** 1324–9